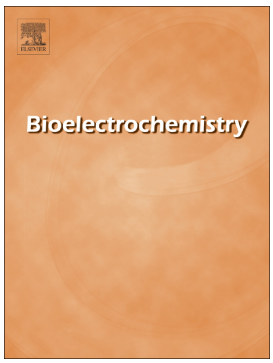

A multi-functional minimally-disruptive portable electrochemical system based on yeast/Co3O4/Au/SPEs for blood lead (II) measurement

Jing Nie, Bin He, Yu-jiao Zang, Wei Yin, Liang-ri Han, Wen-fei Li, Chang-jun Hou, Dan-qun Huo, Mei Yang, Huan-bao Fa

PII: S1567-5394(18)30510-3
DOI: https://doi.org/10.1016/j.bioelechem.2018.12.008
Reference: BIOJEC 7236

To appear in: *Bioelectrochemistry*

Received date: 4 November 2018
Revised date: 19 December 2018
Accepted date: 19 December 2018

Please cite this article as: Jing Nie, Bin He, Yu-jiao Zang, Wei Yin, Liang-ri Han, Wen-fei Li, Chang-jun Hou, Dan-qun Huo, Mei Yang, Huan-bao Fa , A multi-functional minimally-disruptive portable electrochemical system based on yeast/Co3O4/Au/SPEs for blood lead (II) measurement. Biojec (2018), https://doi.org/10.1016/j.bioelechem.2018.12.008

A multi-functional minimally-disruptive portable electrochemical system based on yeast/Co_3O_4/Au/SPEs for blood lead (II) measurement

Jing Nie[1], Bin He[1], Yu-jiao Zang[1], Wei Yin[1]*, Liang-ri Han[1], Wen-fei Li[1], Chang-jun Hou[2], Dan-qun Huo[2] , Mei Yang[2], Huan-bao Fa[1]*

1 National-municipal Joint Engineering Laboratory for Chemical Process Intensification and Reaction, School of Chemistry and Chemical Engineering, Chongqing University, Chongqing 400044, P. R. China.

2 Key Laboratory of Biorheology Science and Technology, Ministry of Education, School of Bioengineering, Chongqing University, Chongqing 400044, P.R. China.

** Corresponding authors.*

E-mail addresses: huanbaofa@cqu.edu.cn (H. Fa), yinweicqu@163.com (W. Yin).

Telephone: +86 13228612804. Fax: +86 23 65102531.

Abstract

A minimally-disruptive portable electrochemical system is constructed by combining a hand-held syringe as reservoir with disposable screen-printed electrodes (SPEs) modified with a simple and efficient yeast/Co_3O_4/Au material for lead determination by a square-wave voltammetry (SWV) method. Not only can it preserve the operation and advantages of the conventional electrochemical procedure, but it also integrates sampling, filtering and analysis to make the determination of lead convenient and effective at higher and lower concentration levels. This is the first report of a microbial biosensor based on active yeast crosslinked to Co_3O_4/Au particles using glutaraldehyde as the crosslinking agent. The determination process is simplified by introducing a fiber filter and takes only 150 seconds with the developed system, which illustrates its simplicity, speed and detection accuracy. Also, the design shows a wide log-linear dynamic range (LDR) from 10^{-8} to 10^{-14} g·L^{-1}, with a limit of detection (LOD) of 3.45×10^{-15} g·L^{-1} (*S*/*N*=3). Additionally, the proposed system was used to determine lead in blood samples, which demonstrated the potential of this biosensor for use in practical applications. Furthermore, this study provides a basis for the development of microscale blood devices for lead measurement.

Keywords: yeast; portable electrochemical system; nano-Co_3O_4/Au; lead determination.

1. Introduction

In recent years, there has been an increasing awareness of the importance of establishing a practical biosensor for blood lead measurement since it is hazardous to human health, especially the high burden on the central nervous system in children [1]. Growth in manufacturing and industrial activities has led to a dramatic increase in lead pollution [2]. Consequently, lead has been recognized as one of the priority pollutants in the environment when its concentration is higher than the international threshold [1, 2].

The development of a miniaturized analytical device has received significant interest to reduce the synthesis and analysis dosage of toxic reagents [3]. Several powerful analytical techniques have been recognized as potential environmentally friendly methods for blood lead determination, such as atomic absorption spectroscopy [4], inductively coupled plasma mass spectroscopy [5], flame atomic absorption spectrometry [6], and graphite furnace atomic absorption spectrometry [7], etc. Despite their considerable advantages, the abovementioned methods are associated with high cost and complex device operation or relatively numerous chemical samples and extended analysis time required. Consequently, bio-electrochemical sensing methods, such as cell-based sensors, enzyme-based sensors, DNA-based sensors, and immunosensors with comparable selectivity and sensitivity, have been proposed to minimize these drawbacks through fast detection, numerical accuracy, and on site environmental emergency assay [8-12]. Tag et al. [13] developed a whole cell-based biosensor by combining saccharomyces cerevisiae cells with Flow Injection Analysis (FIA) for Cu^{2+} determination in the concentration range between 0.05 and 0.35 $mg \cdot L^{-1}$. Zhou et al. [14] developed a highly sensitive electrochemical sensor for Pb^{2+} measurement using an Au-nanoparticle-modified paper working electrode as sensor platform and DNA functionalized iron-porphyrin metal-organic framework nanocomposites as signal probes. In addition, miniature, portable and simple electroanalytical devices are also widely used in blood lead samples actuation and application [15].

Screen-printed electrodes (SPEs) have been used in the field of electrochemical sensing since 1950 due to their well-known advantages for on-site application and use of micro-volumes of the samples [16-19]. The versatile sensing nature of SPEs (e.g., single-use disposable, *in-situ* analysis, simple) is due to the ease with which their surface can be modified by coating with nanomaterials, enzymes, cells, polymers, and complex organic agents [19-22]. Yeast as a multi-functional component of biomass has wide physicochemical tolerances (e.g., pH, temperature, ionic strength), fast growth on different materials, diverse functional groups (e.g.,

amine, hydroxyl, carboxylic), a variety of industrial advantages (e.g., cost-effective, easy accessibility, eco-friendly) and has been successfully used as a biosorbent for Ag^{+}, Cu^{2+}, Pb^{2+}, and Cr^{6+} [23-24]. However, to date, there has been no definitive report on the use of yeast as an electrode modifier for Pb^{2+} electrochemical determination. However, due to its weak conductivity, it is worth noting that yeast crosslinked with a high electron transfer metallic nanostructure to form a new composite material has a significant potential enhancing effect on the catalytic ability, signal-to-noise ratio and charging ability [19, 24]. As an important magnetic *p*-type semiconductor metallic nanomaterial, Co_3O_4 exhibits excellent electrochemical performance due to its mesoporous structure, which can promote the infiltration of electrolyte and ion diffusion [25]. Moreover, a great deal of attention has been paid to further improve the performance in the area of sensing by Co_3O_4 materials decorated with gold nanoparticles with the characteristic biological properties of unique band structure, superior activity or selectivity and environmental friendliness [26]. Thus, it is obvious that SPEs modified by yeast cell integrated into Co_3O_4/Au nanostructures may prove to be an interesting candidate for blood lead detection.

However, most electrochemical methods that use an electrochemical workstation are associated with an electrolytic cell whose performance depends on the electrode and electrolyte. Moreover, some of the electrochemical limitations should be addressed as well [27]. The electrolytic cells available in the market have a volume capacity of about 10-250 mL, holding the as-prepared solution and in turn, causing secondary damage if a large dose of electrolyte is used. Surprisingly, there are few reports on the problems to be solved and the application of miniature and portable electrochemical systems for the determination of real targets.

In this study, a minimally-disruptive portable electrochemical system is introduced for the first time. Not only can it preserve the operation and advantages (e.g., sensitivity, accuracy, etc.) of the conventional electrochemical procedure, but it also integrates sampling, filtering and analysis to make the measurement of lead convenient and effective at higher and lower concentration levels (see schematic S1). The test solutions are drawn into the hand-held syringe and passed through the filter at the bottom of the syringe. Then, the electrochemical assay for the signal-amplified detection is completed when a few drops of the test solution touch the disposable SPEs that are inserted into the syringe. The system can be considered as a portable and compact device, which provides an analytical platform with simple operation and low solution consumption. The system is developed for the first time by combining multi-functional yeast/Co_3O_4/Au composite with SPEs, which is then employed in detecting blood lead with a magnified signal at lower concentration levels. The yeast crosslinked to Co_3O_4/Au composite is

designed to be a sensor in which yeast, without preliminary treatment, is responsible for specific capture of Pb^{2+}, and the Co_3O_4/Au material contributes to increase the conductivity, both of which are necessary for the enhanced peak currents. The system has high sensitivity, low limitation, and small sample volume consumption when used in blood lead detection. The preparation process of this system based on the yeast/Co_3O_4/Au composite is depicted in Schematic 1.

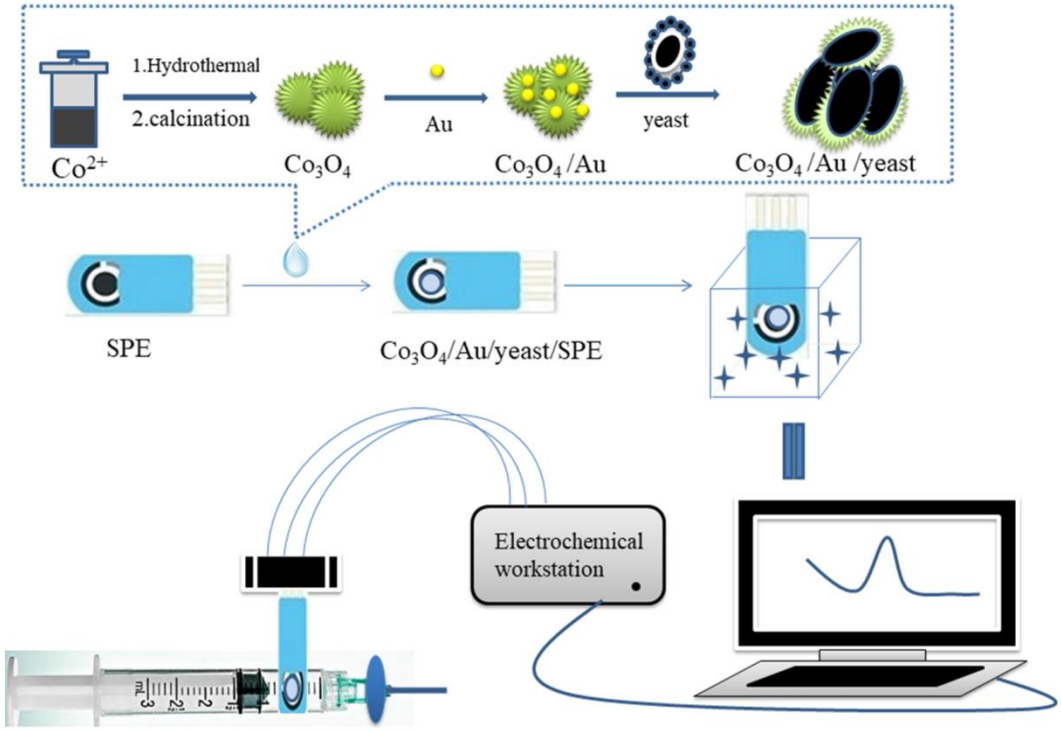

Schematic 1. Preparation process of the minimally-disruptive portable electrochemical system.

2. Experiment

2.1 Preparation of composites

The reagents, instruments, the procedure of synthesis of Co_3O_4, Co_3O_4/Au, yeast/Co_3O_4/Au composites and the preparation of blood samples are described in the Supplementary information (S1).

2.2 Electrochemical testing and construction of the portable electrochemical system

Briefly, the SPEs were scanned by the cyclic voltammograms (n=3) with a range of -1- 0.2 V to check electrochemical performance in 0.1mol·L^{-1} ABS before any electrochemical measurement [28]. 6 μL of the obtained yeast/Co_3O_4/Au suspensions (3 mg yeast/Co_3O_4/Au were dispersed in 3 mL DI water though sonication for 30 min to form 1 mg/mL homogenously suspension) was dipped onto the SPEs surface, dried naturally in air, and denoted as yeast/Co_3O_4/Au/SPEs. Subsequently, square wave voltammogram (SWV) was applied in 0.1 mol·L^{-1} ABS solution containing different concentrations of Pb^{2+} solutions (pH 4.50) for Pb^{2+} assay, with a frequency of 50 Hz, increment potential of 4mV, amplitude of 25 mV, and scan potentials of -1- 0 V.

Construction of the portable system is described in the Supplementary information (S1.4).

3. Result and discussion

3.1 Physicochemical characterization

3.1.1 Scanning electron microscopy

Scanning Electron microscopy (SEM) analysis was performed to observe the morphology of the original yeast, Co_3O_4, Co_3O_4/Au, and yeast cross-linked Co_3O_4/Au composite materials. The image displayed in Fig. 1A reveals that the pure yeast cells appeared as single cells with oval shape, smooth surface, and a length and width of about 5 and 3 μm, respectively [29, 30]. The image presented in Fig. 1B shows that the newly-prepared Co_3O_4 nanomaterial displays a needle flower morphology with an average diameter of about 2 - 5 μm, which are composed of a large number of interconnected nanoparticles. Notably, similar morphology has been observed in Au-decorated Co_3O_4 nanoparticles (Fig. 1C), except that the surface of the needle-like composite is slightly smooth, as the spacing of the petal-like structure is developed by Au nanocomposites. Additionally, the image displayed in Fig. 1D also reveal that the Au-decorated Co_3O_4 nanoparticles are randomly linked on the surface of the yeast though the functional groups on the yeast—NH_2, OH, COOH, etc., which provide numerous adsorption sites for target detection.

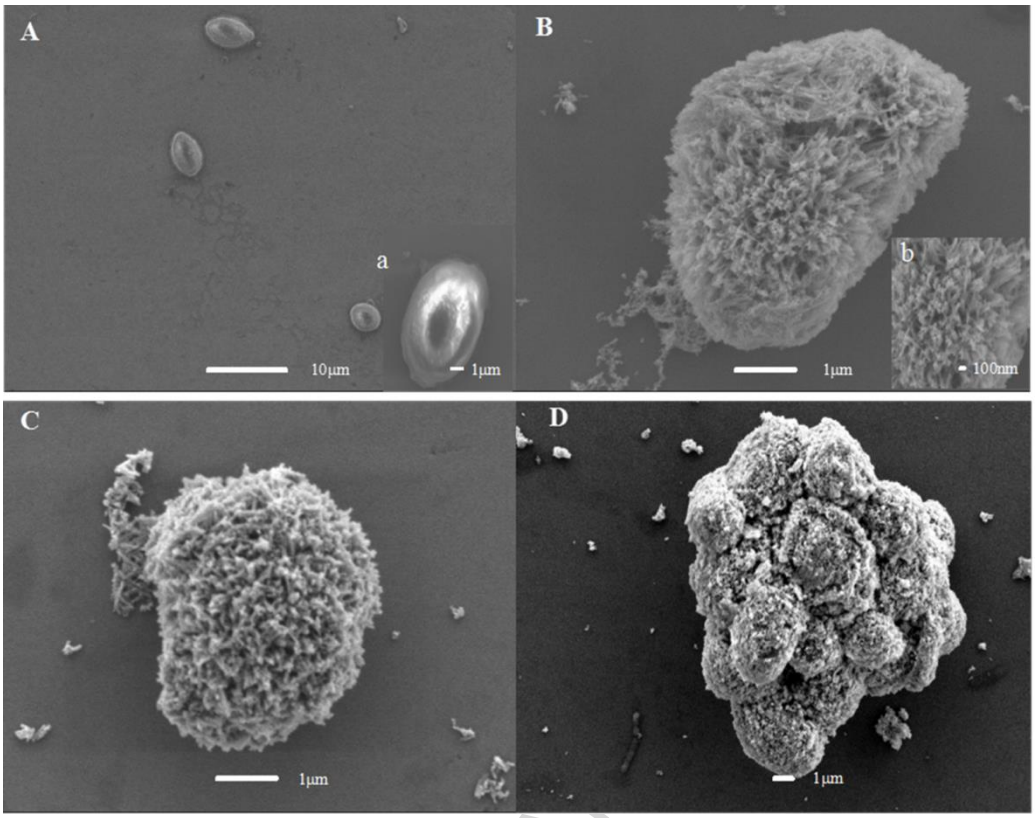

Fig. 1. Scanning electron microscopy (SEM) image of pure yeast cells (A), Co_3O_4 (B), Co_3O_4/Au (C) and yeast/Co_3O_4/Au (D). The insert images of (a) and (b) display the high-magnification of pure yeast and Co_3O_4.

3.1.2 X-ray diffraction

All X-ray diffraction (XRD) patterns are displayed in the Fig. 2. Specifically, in Fig. 2a, the strong peaks that appear at 2θ values of 31.3°, 36.9 °, 44.9°, 59.5°, and 65.3°, according to the spinel structure of Co_3O_4 (JCPDS card no.42-1467) [31], can be ascribed to the crystal planes (220), (311), (400), (511), and (440), respectively. The new peaks observed at 2θ=38.2°, 44.4°, 64.6°, 77.5° are in good agreement with the (111), (200), (220), (311) planes of the cubic Au phase (JCPDS card no.89-3697) [32]. Also, as shown in Fig. 2c, all the diffraction peaks appear to have clearly strengthened, which indicates that Au-decorated Co_3O_4 nanoparticles are associated with the yeast. Thus, the XRD patterns completely confirm the successful synthesis of Co_3O_4, Au-decorated Co_3O_4, and yeast cross-linked Co_3O_4/Au.

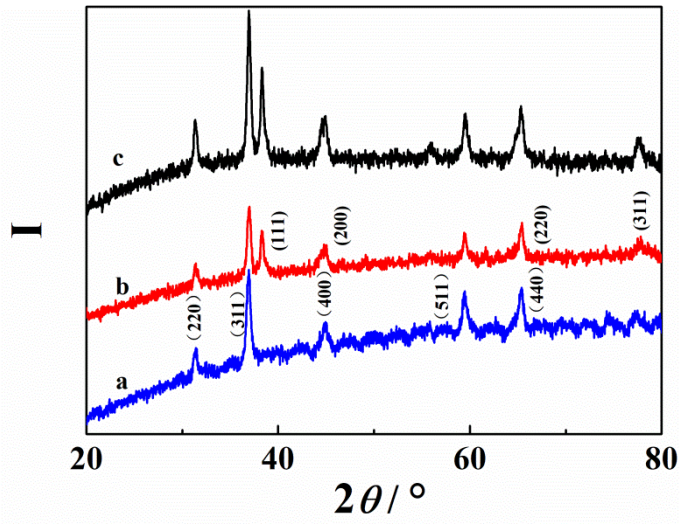

Fig 2. X-ray diffraction (XRD) pattern of (a) Co_3O_4, (b) Co_3O_4/Au and (c) Co_3O_4/Au/yeast.

3.1.3 Fourier transform infrared spectroscopy

The Fourier transform infrared (FTIR) spectroscopy measurements were performed to determine the components of the Co_3O_4, Co_3O_4/Au, yeast cross-linked Co_3O_4/Au, separately. The spectra shown in Fig. 3a and b display broad and strong peaks at 3431.3 and 1636.4 cm^{-1} that correspond to the O-H group stretching vibration, while those at 655.9 and 574.9 cm^{-1} are the characteristic peaks of Co_3O_4. Compared with the spectrum pattern in Fig. 3 a, all the peaks in the spectrum pattern in Fig. 3b are strengthened and sharped without any other obvious change, which indicates that the Au nanomaterial has been successfully anchored on the surface of Co_3O_4. In addition, it is clearly seen that the wide and intense peaks at Fig. 3c display significant alteration due to the introduction of yeast biomass. The flat peak at 3,304.5 cm^{-1} is assigned to the overlapping of the -NH- bending mode of the amino group in proteins or peptides and it might also be associated with the vibration of absorbed water molecules or surface –OH group in yeast. The 1,647.6 cm^{-1} region can be primarily ascribed to C=O stretching, indicating the presence of carboxyl functional groups. The emerging peaks at 1,541.1, 1,045.6, and 1,235.5 cm^{-1} may be respectively attributed to -C=C-, -P=O- and free amino acids stretching vibration originating from the yeast structure, reflecting the successful preparation of the yeast/Co_3O_4/Au material. Two sharp peaks are slightly shifted to the right (～5 cm^{-1}) due to the change of the Co-O bond, which confirms that yeast cells have been crosslinked to the Co_3O_4/Au material. Accordingly, an inference can be drawn that the active functional groups (-NH-, -OH-, -C=O-(-COOH), -C=C-, -P=O-(-OPO_3^{2-})), most of which are the characteristic of yeast, are well-distributed on the composite material and play a vital role in the process of lead absorption.

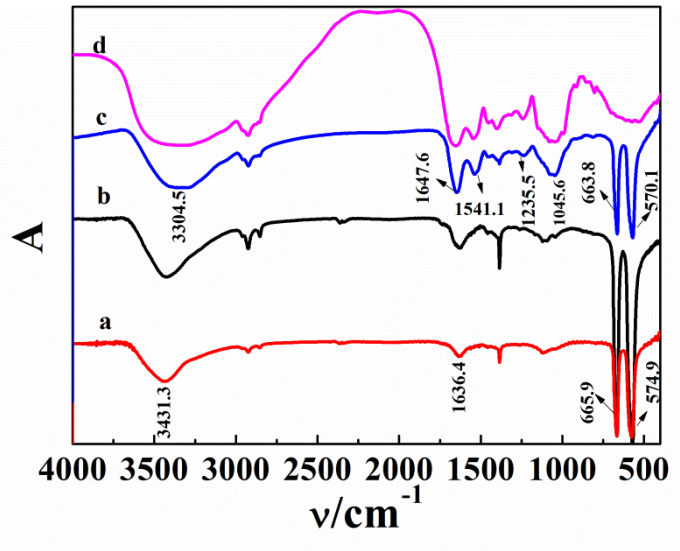

Fig 3. Fourier transform infrared (FTIR) spectra of (a) Co_3O_4, (b) Co_3O_4/Au, (c) Co_3O_4/Au/yeast and (d) pure yeast cells.

3.2 Electrochemical characteristics of a biosensor using minimally-disruptive portable electrochemical system

3.2.1 Basic characteristics of the modified SPEs

The cyclic voltammetry (CV) curves shown in Fig. 4A was recorded to investigate the electrochemical behavior of $[Fe(CN)_6]^{3-}$ in 5.0 mmol·L^{-1} $K_3[Fe(CN)_6]$ containing 0.1 mol·L^{-1} KCl solution. Specifically, the SPEs were modified by Co_3O_4 (curve b), Co_3O_4/Au (curve c), yeast/Co_3O_4/Au (curve d) materials. Compared with curve a (for bare SPEs), the peak currents of all modified SPEs clearly declined at both the cathodic and anodic peaks, which might be due to the decrease of the contact area between the SPEs and electrolyte following the attachment of the composite to the SPEs, which might influence the electron transfer rates [33-34]. At the same time, the shifting of the peaks observed in Fig. 4A can be ascribed to the introduction of the Co_3O_4, Co_3O_4/Au, yeast/Co_3O_4/Au materials, which provide more adsorption sites for target analyte. Besides suggesting inferior conductivity, those phenomena also indicate the higher number of adsorption sites of the yeast/Co_3O_4/Au/SPEs.

In addition, to investigate the electrochemical behavior of 10^{-9} g·L^{-1} of Pb^{2+} in 0.1 M ABS (pH =4.50), the changes in the performance of modified SPEs were explored by the square-wave voltammetry (SWV) methods. The results presented in Fig. 4B reveal that after introduction of Co_3O_4 (curve b), the peak currents that are dramatically enhanced can be ascribed to the mesoporous structure of Co_3O_4. Additionally, curve d shows that the peak currents with

Co_3O_4/Au/SPEs are increased compared to those with Co_3O_4/SPEs due to the satisfactory conductivity of Au nanoparticles. The yeast/Co_3O_4/Au/SPEs clearly exhibit slightly higher current values compared with those of Co_3O_4/Au/SPEs, indicating that the Co_3O_4/Au material is well anchored on the yeast cells. The significantly increased values for the current of yeast/Co_3O_4/Au/SPEs imply that such material can be used as a promising sensor to enhance the chemical sensitive for target assay.

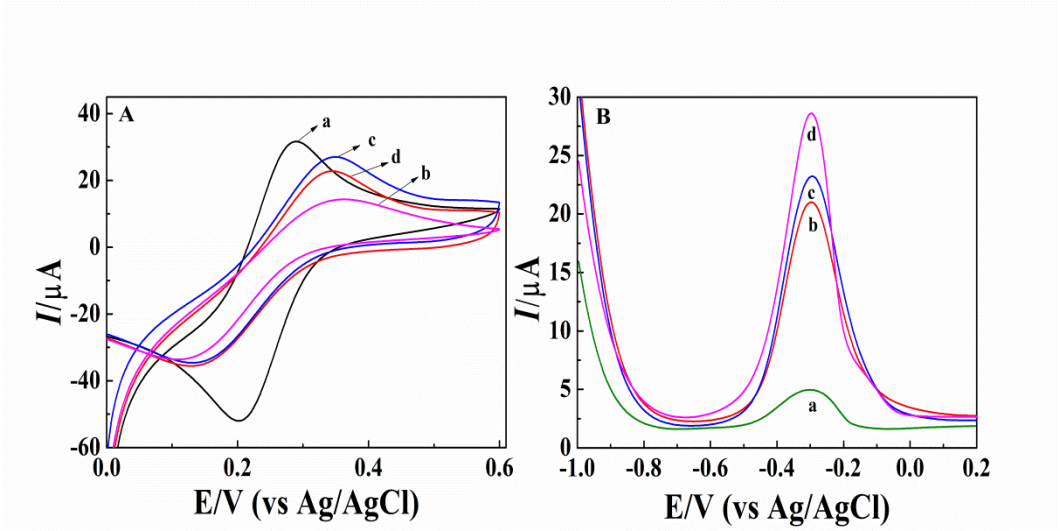

Fig. 4. Cyclic voltammetry (CV) curves of (A) and SWV curves of (B) of (a) bare SPEs, (b) Co_3O_4/SPEs, (c) Co_3O_4/Au/SPEs and (d) Co_3O_4/Au/yeast/SPEs.

3.2.2 Optimization of assay conditions

The assay conditions of pH, time, and volume were optimized and are described in the Supplementary Information (S2.1). In total, the optimum experimental conditions were as follows: the pH of the supporting electrolyte solution was 4.50, pre-concentration time was 150 s, and loading volume was 6 μL.

3.2.3 Electrochemical response to lead

Under the optimized conditions, the lead measurements by the SWV method were performed by using the system prepared with yeast/Co_3O_4/Au/SPEs in 0.1 M ABS. The response concentration of Pb^{2+} and the calibration plot are shown in Fig. 5, which surprisingly reveal that the electrochemical responses to Pb^{2+} in the concentration range of 10^{-8} g·L^{-1} to 10^{-14} g·L^{-1} exhibited increasing current. In other words, the magnitude of the peak currents increased proportionally with the decrease in the concentration of Pb^{2+}, which can be attributed to the inhibitory effect of the high concentration of Pb^{2+} on the yeast cells [35-37]. Meanwhile, the slight

shift to the right of the peak currents in Fig. 5A can be related to the materials adsorbed onto the electrodes and the difference in the nature of lead solutions [38-39]. The resulting calibration plot could be represented as y=38.8261-5.09947 lg *C* (*C*: pg·L^{-1}, y: μA) with a correlation coefficient of 0.99783. The limit of detection (LOD) and limit of quantification (LOQ) were calculated as 3.45×10^{-15} g·L^{-1} (*S*/*N*=3) and 1.15×10^{-14} g·L^{-1} (*S*/*N*=10), respectively, which were considerably lower than the recommended value of 10^{-2} g·L^{-1} for Pb^{2+} in children's blood. The inhibitory effect of the high concentration of Pb^{2+} on yeast cells was further investigated, as shown in Fig. S2, by increasing the Pb^{2+} concentration, the electrochemical signals are increased inversely in the range of 10^{-7}-10^{-3} g·L^{-1}, which indicates that a certain amount of Pb^{2+} had accumulated on the surface of the yeast cells, so that they becomes inactivated. In this case, inactivated yeast cells have a weaker ability to contribute to the electrochemical signal. Thus, it can be inferred that the changes of the peak currents in Fig. S2 are mainly dependent on the conductivity of the Co_3O_4/Au composite. Meanwhile, the phenomenon depicted in Fig. 5 indicates that combining yeast cells with Co_3O_4/Au materials has a synergistic effect on the signal-enhanced detection, and an increase of the number of active yeast cells or yeast metabolites do promote the signal generation [40-43]. Our work shows that the developed system has a wide log-linear range and a low detection limit with a negatively correlated relationship between the peak currents and the concentrations of Pb^{2+} at lower concentration levels, and it is also better than other previously reported methods. A detailed comparison with analytical performance and modified electrode is given in Table 1.

Also, the reproducibility and stability of the biosensor are illustrated in the Supplementary Information (S2.2). The reproducibility has a satisfactory relative standard deviation (RSD) of 1.25% for peak currents and the loss of the peak currents is about 5% of the initial response during two weeks.

In addition, interfering ions, such as Co^{2+}, Ni^{2+}, Fe^{3+}, Cu^{2+}, Ag^{+}, Mn^{2+}, Zn^{2+}, Hg^{2+}, Cr^{6+} and Cd^{2+}, were introduced to evaluate the interference with 10^{-9} g·L^{-1} Pb^{2+} under optimal conditions. The addition of 1,000-fold excess concentration of Cl^{-}, SO_4^{2-}, NO_3^{-}, and PO_4^{3-} resulted in barely any interference with Pb^{2+} ions. The results shown in Fig. 6 reveal that the deviation of the peak currents is within 5% after the addition of 50-fold concentration of Co^{2+}, Ni^{2+}, Fe^{3+}, and Mn^{2+}. Also, a 20-fold excess concentration of Ag^{+}, Cr^{6+}, Cd^{2+} and Zn^{2+} caused a decrease in the peak currents of approximately 11%, as a result of the multi-functional (-NH-, -OH-, -P=O-) adsorption capacity of yeast cells. However, due to the formation of intermetallic compounds at a concentration of about 10-fold Cu^{2+} and Pb^{2+}, the peak currents decreased 19%. On the other hand, a concentration of 10-fold Hg^{2+} has the capacity to promote the formation of mercury film, with

the stripping peak currents rising about 7%. This result basically indicates a significant effect of the presence of the eleven co-ions on lead determination.

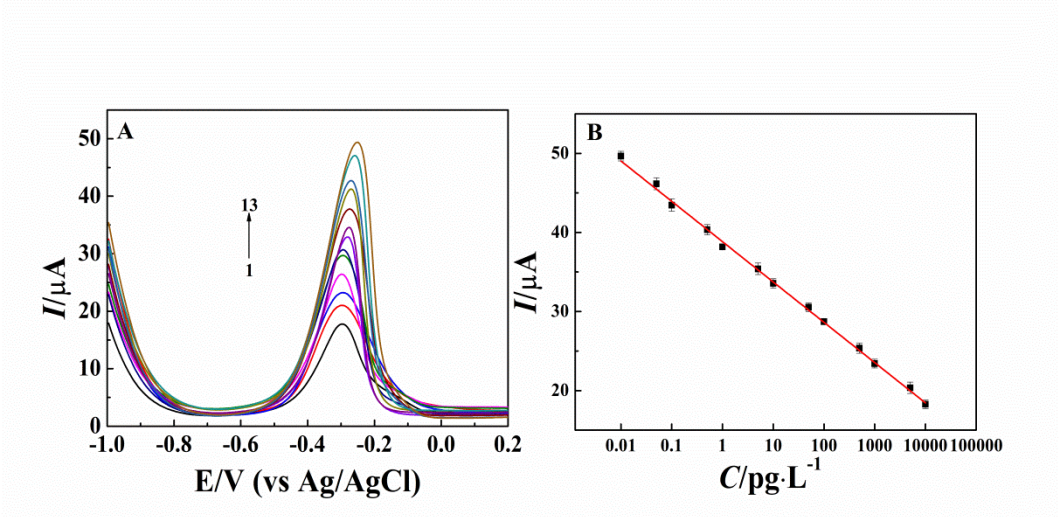

Fig. 5. (A) SWV response currents of Co_3O_4/Au/yeast/SPEs in 0.1 M ABS (pH=4.50) containing different Pb^{2+} concentration (1-13)：0.01, 0.05, 0.1, 0.5, 1, 5, 10, 50, 100, 500, 1000, 5000 and 10000 pg·L^{-1}. Plot of the peak currents against the concentration of Pb^{2+} was shown in Fig. 5B and the calibration plot could be represented as y=38.8261-5.09947 lg *C* (*C*: pg·L^{-1}, y: μA) with a correlation coefficient of 0.99783. Error bar: n=3.

Table 1 Comparison of analytical properties of different modified electrodes toward Pb^{2+}.

Electrodes	Methods	LDR(g·L^{-1})	LOD(g·L^{-1})	References
Bi^{3+}/SPEs	DPV	2.1×10^{-4}-2.1×10^{-3}	2.1×10^{-6}	[44]
Hg-coated SPEs	ASV	6.3×10^{-6}-5.0×10^{-4}	9×10^{-7}-1.5×10^{-6}	[45]
STV- PbS QDs/SPEs	ASV	2.0×10^{-7}- 10^{-4}	5×10^{-8}	[46]
Ph-COOH-AuNPs/SPEs	SWASV	5.2×10^{-7} -5.2×10^{-6}	-	[47]
Gold-based SPEs	SWASV	10^{-6}-10^{-3}	3×10^{-7}	[48]
diazonium salts/SPEs	SWASV	7.0×10^{-8} - 5.2×10^{-5}	2×10^{-8}	[49]
Bi_2O_3/SPEs	SWASV	0-1.2×10^{-5}	2×10^{-7}	[50]
Bi/SPE	SWASV	10^{-5} -10^{-4}	4×10^{-6}	[51]
mPMF-modified SPEs	SWV	10^{-6}-5×10^{-5}	10^{-7}	[52]
EDTA_PANI/SWCNTs/SS	DPV	4.1×10^{-4}-7.7×10^{-3}	3.4×10^{-4}	[53]
EDTA-Ppy/SWNTs/SSE	CV	3.1×10^{-5}-0.17	1.5×10^{-5}	[54]
Yeast/Co_3O_4/Au/SPEs	SWV	10^{-8}-10^{-14}	3.45×10^{-15}	This work

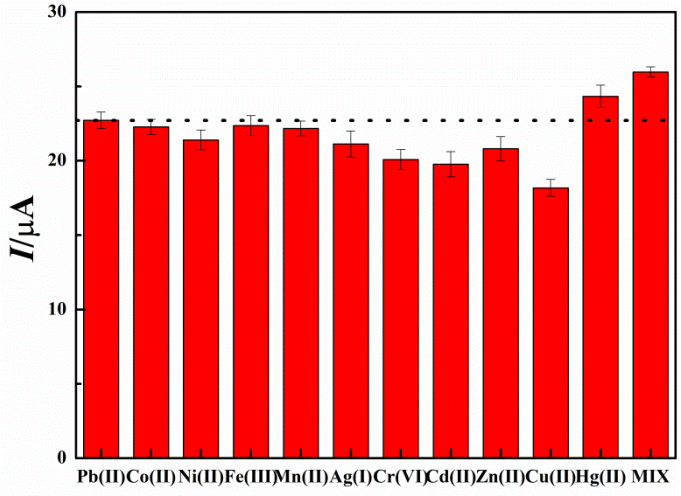

Fig. 6. Anti-interference ability of prepared system in the presence of 1×10^{-9} g·L^{-1} Pb^{2+} and other heavy metal ions(5×10^{-8} g·L^{-1} Co^{2+}, 5×10^{-8} g·L^{-1} Ni^{2+}, 5×10^{-8} g·L^{-1} Fe^{3+}, 5×10^{-8} g·L^{-1} Mn^{2+}, 2×10^{-8} g·L^{-1} Ag^{+}, 2×10^{-8} g·L^{-1} Cr^{6+}, 2×10^{-8} g·L^{-1} Cd^{2+}, 2×10^{-8} g·L^{-1} Zn^{2+}, 10^{-8} g·L^{-1} Cu^{2+}, 10^{-8} g·L^{-1} Hg^{2+}). Error bar: n=3.

3.3 Application of the minimally-disruptive portable electrochemical system for lead detection in blood samples

The practical feasibility of the application of the developed system for lead detection was evaluated in blood serum samples by recovery tests. The data listed in Table 2 are the results determined by the SWV method using the developed system after the addition of 0, 5×10^{-9}, 5×10^{-13} g·L^{-1} Pb^{2+}. Compared with the standard value, the actual measured value is obtained from the calibration plot after deducting the blank dissolution peak currents. The recovery rate of the samples ranged from 97.28-109.41%, indicating that the system is not influenced by the presence of serum components and has a high potential for application in blood lead determination.

To illustrate the possible application of this system, the venous blood samples were collected into tubes containing the anticoagulant sodium heparin and centrifuged at 4,000 rpm for 8 minutes to obtain the serum sample 3 (the pale yellow supernatant). One drop of the serum samples was directly diluted 20 fold with a 0.1 M acetate buffered saline (ABS) solution (pH 4.5), using a special syringe. The obtained suspension could be used in subsequent analysis without any further treatment. Pb^{2+} was detected by the standard addition method. A certain amount of Pb^{2+} was added to the suspension to prepare the simulated blood serum samples. The results in sample 3 revealed

that the RSD values were less than 5% for all samples with an excellent percentage recovery, close to 100%, indicating that the system can efficiently detect lead in blood and serum samples.

Table 2 Determination of Pb^{2+} recovery by the suggested sensor in different blood samples ($g \cdot L^{-1}$).

Samples	Pb^{2+} Added	Pb^{2+} Found [a]	Recovery(%)	RSD(%)
1 (serum sample)	0	n.q.	--	4.33
	5×10^{-13}	$(4.86\pm0.79)\times10^{-13}$	97.28±0.16	2.72
	5×10^{-9}	$(5.35\pm0.87)\times10^{-9}$	107.14±0.17	3.09
2 (serum sample)	0	n.q.	--	4.79
	5×10^{-13}	$(5.47\pm0.43)\times10^{-13}$	109.41±0.086	2.64
	5×10^{-9}	$(5.09\pm1.02)\times10^{-9}$	101.89±0.20	3.59
3 (blood sample)	0	0.0297±0.032	--	3.18
	5×10^{-13}	$(5.12\pm0.56)\times10^{-13}$	102.42±0.112	3.45
	5×10^{-9}	$(4.93\pm0.35)\times10^{-9}$	98.61±0.07	3.31

[a] Average of three replicate measurements.

n.q.: not quantified.

4. Conclusions

In this paper, the fabrication of a minimally-disruptive portable electrochemical system using a multi-functional yeast/Co_3O_4/Au sensor for the rapid identification of lead in blood serum samples is described for the first time. Due to the integration of the sampling, filtering and analysis, the determination of lead with this newly developed system is convenient, and effective at higher and lower lead concentration levels. The design can not only take full advantage of the electrochemical sensing methods, but also reduce the amount of electrolyte and optimize materials loading on electrodes for ultra-trace analysis of lead in blood. The results also revealed a negative relationship between the concentration of lead and the peak current signal at lower concentration levels. Additionally, the results also showed a wide log-linear range, low detection limit, good reproducibility and stability, and acceptable recovery rate. In summary, the developed sensor used in the newly developed system for lead analysis is simple in operation, easy to manufacture, highly reliable, and cost-effective in materials, opening a new perspective in the rapid detection of lead.

Acknowledgements

This work was supported by the National Natural Science Foundation of China (31101284), Chongqing science and technology commission (cstc2015shmszxl20097, cstc2017shmsA100010), the Graduate Research and Innovation Foundation of Chongqing, China (No.CYS17017) and the Chongqing University Student Research Training Program (No. CQU-SRTP-2018336 and CQU-SRTP-2018348).

Reference

[1] G. Markowitz, The childhood lead poisoning epidemic in historical perspective, Endeavour 40 (2016) 93-101. 10.1016/j.endeavour.2016.03.006.

[2] S. Hernberg MD PhD, Lead poisoning in a historical perspective, Am. J. Ind. Med. 38 (2010) 244-54. 10.1002/1097-0274(200009)38:3<244::AID-AJIM3>3.0.CO;2-F.

[3] W.R. Melchert, F.R. Rocha, A green analytical procedure for flow-injection determination of nitrate in natural waters, Talanta 65 (2005) 461-5. https://doi.org/10.1016/j.talanta.2004.06.022.

[4] H.İ. Ulusoy, Ü. Aksoy, M. Akçay, Simultaneous pre-concentration of Pb and Sn in food samples and determination by atomic absorption spectrometry, Eur. Food Res. Technol. 236 (2013) 725-733. https://doi.org/10.1007/s00217-013-1929-6.

[5] H.R. Kuhn, D. Gunther, Elemental Fractionation Studies in Laser Ablation Inductively Coupled Plasma Mass Spectrometry on Laser-Induced Brass Aerosols, Anal. Chem. 75 (2003) 747-753. 10.1021/ac0259919.

[6] E. Yavuz, Ş. Tokalıoğlu, H. Şahan, Ş. Patat, Nanosized spongelike Mn_3O_4 as an adsorbent for preconcentration by vortex assisted solid phase extraction of copper and lead in various food and herb samples, Food Chem. 194 (2016) 463-469. https://doi.org/10.1016/j.foodchem.2015.08.035.

[7] W.S. Zhong, T. Ren, L.J. Zhao, Determination of Pb (Lead), Cd (Cadmium), Cr (Chromium), Cu (Copper), and Ni (Nickel) in Chinese tea with high-resolution continuum source graphite furnace atomic absorption spectrometry, J. Food Drug Anal. 24 (2016) 46-55. 10.1016/j.jfda.2015.04.010.

[8] Q. Liu, H. Cai, Y. Xu, L. Xiao, M. Yang, P. Wang, Detection of heavy metal toxicity using cardiac cell-based biosensor, Biosens. Bioelectron. 22 (2007) 3224-3229. https://doi.org/10.1016/j.bios.2007.03.005.

[9] X. Zhu, G. Wu, N. Lu, X. Yuan, B. Li, A miniaturized electrochemical toxicity biosensor based on graphene oxide quantum dots/carboxylated carbon nanotubes for assessment of priority pollutants, J. Hazard. Mater. 324 (2016) 272-280. https://doi.org/10.1016/j.jhazmat.2016.10.057.

[10] Y. Song, Y. Luo, C. Zhu, H. Li, D. Du, Recent advances in electrochemical biosensors based on graphene two-dimensional nanomaterials, Biosens. Bioelectron. 76 (2016) 195-212. https://doi.org/10.1016/j.bios.2015.07.002.

[11] J. Zhuang, L. Fu, M. Xu, Q. Zhou, G. Chen, D. Tang, DNAzyme-based magneto-controlled electronic switch for picomolar detection of lead (II) coupling with DNA-based hybridization chain reaction, Biosens. Bioelectron. 45 (2013) 52-57. https://doi.org/10.1016/j.bios.2013.01.039.

[12] X.X. Dong, J.Y. Yang, L. Luo, Y.F. Zhang, C. Mao, Y.M. Sun, H.T. Lei, Y.D. Shen, R.C. Beier, Z.L. Xu, Portable amperometric immunosensor for histamine detection using Prussian blue-chitosan-gold nanoparticle nanocomposite films, Biosens. Bioelectron. 98 (2017) 305-309. https://doi.org/10.1016/j.bios.2017.07.014.

[13] K. Tag, K. Riedel, H.J. Bauer, G. Hanke, K.H.R. Baronian, G. Kunze, Amperometric detection of Cu^{2+} by yeast biosensors using flow injection analysis (FIA), Sens. Actuators B: Chem. 122 (2007) 403-409. https://doi.org/10.1016/j.snb.2006.06.007.

[14] X. Wang, C. Yang, S. Zhu, M. Yan, S. Ge, J. Yu, 3D origami electrochemical device for sensitive Pb^{2+} testing based on DNA functionalized iron-porphyrinic metal-organic framework, Biosens. Bioelectron. 87 (2017) 108-115. https://doi.org/10.1016/j.bios.2016.08.016.

[15] J.C. Quintana, F. Arduini, A. Amine, K.V. Velzen, G. Palleschi, D. Mosconeab, Part two: Analytical optimisation of a procedure for lead detection in milk by means of bismuth-modified screen-printed electrodes, Anal. Chim. Acta 736 (2012) 92-99. https://doi.org/10.1016/j.aca.2012.05.042.

[16] G.M. Ferrari, O. Amor-Gutiérrez, E. Costa-Rama, M.T. Fernández-Abedul, Batch injection electroanalysis with stainless-steel pins as electrodes in single and multiplexed configurations, Sens. Actuators B: Chem. 253 (2017) 1207-1213. https://doi.org/10.1016/j.snb.2017.07.148.

[17] D.M. Cate, J.A. Adkins, J. Mettakoonpitak, C.S. Henry, Recent developments in paper-based microfluidic devices, Anal. Chem. 87 (2015) 19-41. 10.1021/ac503968p.

[18] S.T. Sanjay, G. Fu, M. Dou, F. Xu, R. Liu, H. Qi, X. Li, Biomarker detection for disease diagnosis using cost-effective microfluidic platforms, Analyst. 140 (2015) 7062-7081.

10.1039/c5an00780a.

[19] S.A. Tukur, N.A. Yusof, R. Hajian. Linear sweep anodic stripping voltammetry: Determination of Chromium (VI) using synthesized gold nanoparticles modified screen-printed electrode, J. Chem. Sci. 127 (2015) 1-7. https://doi.org/10.1007/s12039-015-0864-4.

[20] N. Promphet, P. Rattanarat, R. Rangkupan, O. Chailapakul, N. Rodthongkum, An electrochemical sensor based on graphene/polyaniline/polystyrene nanoporous fibers modified electrode for simultaneous determination of lead and cadmium, Sens. Actuators B: Chem. 207 (2015) 526-534. https://doi.org/10.1016/j.snb.2014.10.126.

[21] N.A. Rahman, N.A. Yusof, N.A.M. Maamor, S.M.M. Noor, Development of Electrochemical Sensor for Simultaneous Determination of Cd(II) and Hg(II) Ion by Exploiting Newly Synthesized Cyclic Dipeptide, Int. J. Electrochem. Sci. 7 (2017) 186-196. http://orcid.org/0000-0002-1400-5764.

[22] N. Daud, N.A. Yusof, W.T. Tan, Development of Electrochemical Sensor for Detection of Mercury by Exploiting His-Phe-His-Ala-His-Phe-Ala-Phe Modified Electrode, Int. J. Electrochem. Sci. 6 (2011) 2798-2807. http://orcid.org/0000-0002-1400-5764.

[23] F. Lagarde, N. Jaffrezic-Renault, Cell-based electrochemical biosensors for water quality assessment, Anal. Bioanal. Chem. 400 (2011) 947-964. 10.1007/s00216-011-4816-7.

[24] W. Zhang, L. Meng, G. Mu, M. Zhao, P. Zou, Y. Zhang, A facile strategy for fabrication of nano-ZnO/yeast composites and their adsorption mechanism towards lead (II) ions, App. Surf. Sci. 378 (2016) 196-206. 10.1016/j.apsusc.2016.03.215.

[25] S. Xiong, C. Yuan, X. Zhang, B. Xi, Y. Qian, Controllable synthesis of mesoporous Co_3O_4 nanostructures with tunable morphology for application in supercapacitors, Chem. Eur. J. 15 (2009) 5320-5326. 10.1002/chem.200802671.

[26] Y. Ma, S. Qing, Z. Gao, X. Mamat, J. Zhang, H. Li, W. Eli, T. Wang, Tandem hydroformylation and hydrogenation of dicyclopentadiene by Co_3O_4 supported gold nanoparticles, Catal. Sci. Technol. 5 (2015) 3649-3657. http://orcid.org/0000-0002-8213-4314.

[27] D. Ji, L. Liu, S. Li, C. Chen, Y. Lu, J. Wu, Q. Liu, Smartphone-based cyclic voltammetry system with graphene modified screen printed electrodes for glucose detection, Biosens. Bioelectron. 98 (2017) 449-456. https://doi.org/10.1016/j.bios.2017.07.027.

[28] M. Carbone, A. Nesticò, N. Bellucci, L. Micheli, G. Palleschi, Enhanced performances of sensors based on screen printed electrodes modified with nanosized NiO particles, Electrochim. Acta. 246 (2017) 580-587. 10.1016/j.electacta.2017.06.074.

[29] T. Sathvika, Manasi, V. Rajesh, N. Rajesh, Microwave assisted immobilization of yeast in cellulose biopolymer as a green adsorbent for the sequestration of chromium, Chem. Eng. J. 279 (2015) 38-46. 10.1016/j.cej.2015.04.132.

[30] W. Zhang, F. Wang, P. Wang, L. Lin, Y. Zhao, P. Zou, M. Zhao, H. Chen, Y. Liu, Y. Zhang, Facile synthesis of hydroxyapatite/yeast biomass composites and their adsorption behaviors for lead (II), J. Colloid Interf. Sci. 477 (2016) 181-190. 10.1016/j.jcis.2016.05.050.

[31] P. Liu, Q. Hao, X. Xia, L. Lu, W. Lei, X. Wang, 3D Hierarchical Mesoporous Flowerlike Cobalt Oxide Nanomaterials: Controllable Synthesis and Electrochemical Properties, J. Phys. Chem. C 119 (2015) 8537-8546. 10.1021/acs.jpcc.5b01315.

[32] S. Ma, Q. Cai, K. Lu, F. Liao, M. Shao, Bi-functional Au/FeS (Au/Co_3O_4) composite for in situ SERS monitoring and degradation of organic pollutants, J. Nanopart. Res. 18 (2016) 1-13. 10.1007/s11051-016-3335-z.

[33] P.H. Li, Y.X. Li, S.H. Chen, S.S. Li, M. Jiang, Z. Guo, J.H. Liu, X.J. Huang, M. Yang, Sensitive and interference-free electrochemical determination of Pb(II) in wastewater using porous Ce-Zr oxide nanospheres, Sens. Actuators B: Chem. 257 (2018) 1009-1020. 10.1016/j.snb.2017.11.061.

[34] F.R. Caetanoa, E.A. Carneiroa, D. Agustinia, L.C.S. Figueiredo-Filhob, C.E. Banksc, M.F. Bergaminia, L.H. Marcolino-Juniora, Combination of electrochemical biosensor and textile threads: Amicrofluidic device for phenol determination in tap water, Biosens. Bioelectron. 99 (2018) 382-388. 10.1016/j.bios.2017.07.070.

[35] L. Flórez-Miranda, R.O. Cañizares-Villanueva, O. Melchy-Antonio, F. Martínez-Jerónimo, C.M. Flores-Ortíz, Two stage heterotrophy/photoinduction culture of Scenedesmus incrassatulus: potential for lutein production, J. Biotechnol. 262 (2017) 67-74. http://orcid.org/0000-0003-1484-9817.

[36] V.A. Mesquita, M.D. Machado, C.F. Silva, E.V. Soares, Impact of multi-metals (Cd, Pb and Zn) exposure on the physiology of the yeast Pichia kudriavzevii, Environ. Sci. Pollut. Res. 22 (2015) 11127-11136. 10.1007/s11356-015-4326-9.

[37] X. Sun, Y. Zhao, L. Liu, B. Jia, F. Zhao, W. Huang, J. Zhan, Copper Tolerance and Biosorption of Saccharomyces cerevisiae during Alcoholic Fermentation, Plos One, 10 (2015) e0128611. 10.1371/journal.pone.0128611.

[38] L. Wang, W.H. Xu, R. Yang, T. Zhou, D. Hou, X. Zheng, J.H. Liu, X.J. Huang, Electrochemical and density functional theory investigation on high selectivity and sensitivity of exfoliated nano-zirconium phosphate toward lead(II), Anal. Chem. 85

(2013) 3984-3990. http://orcid.org/0000-0003-3310-7675.

[39] L.A. Hutton, M.E. Newton, P.R. Unwin, J.V. Macpherson, Factors controlling stripping voltammetry of lead at polycrystalline boron doped diamond electrodes: new insights from high-resolution microscopy, Anal. Chem. 83 (2011) 735-745. 10.1021/ac101626s.

[40] J. Posseckardt, C. Schirmer, A. Kick, K. Rebatschek, T. Lamz, M. Mertig, Monitoring of Saccharomyces cerevisiae viability by non-Faradaic impedance spectroscopy using interdigitated screen-printed platinum electrodes, Sens. Actuators B: Chem. 255 (2018) 3417-3424. 10.1016/j.snb.2017.09.171.

[41] B. Liu, Y. Lei, B. Li, A batch-mode cube microbial fuel cell based “shock” biosensor for wastewater quality monitoring, Biosens. Bioelectron. 62 (2014) 308-314. http://orcid.org/0000-0002-6825-3536.

[42]X. Zhang, X. Zhang, W. He, C. Sun, J. Ma, J. Yuan, X. Du, High-performance mesoporous $LiFePO_4$ from Baker's yeast, Colloids and Surfaces B: Biointerfaces 103 (2013) 114-120. 10.1016/j.colsurfb.2012.10.002.

[43] E.T. Kasem, T. Tsujiguchi, N. Nakagawa, Kasem, Effect of Metal Modification to Carbon Paper Anodes on the Performance of Yeast-Based Microbial Fuel Cells Part I: In the Case without Exogenous Mediator, Key Engineering Materials.534 (2013) 76-81. https://doi.org/10.4028/www.scientific.net/KEM.534.76.

[44] M. Li, D.W. Li, Y.T. Li, D.K. Xu, Y.T. Long, Highly selective in situ metal ion determination by hybrid electrochemical "adsorption-desorption" and colorimetric methods, Anal. Chim. Acta 701 (2011) 157-163. 10.1016/j.aca.2011.06.016.

[45] F. Fan, J. Dou, A. Ding, K. Zhang, Y. Wang, Determination of lead by square wave anodic stripping voltammetry using an electrochemical sensor, Anal. Sci. 29 (2013) 571-577. 10.2116/analsci.29.571.

[46] C. Kokkinos, M. Prodromidis, A. Economou, P. Petro, S. Kakabakos, Disposable integrated bismuth citrate-modified screen-printed immunosensor for ultrasensitive quantum dot-based electrochemical assay of C-reactive protein in human serum, Anal. Chim. Acta. 886 (2015) 29-36. https://doi.org/10.1016/j.aca.2015.05.035.

[47] J.P. Jasmin, C. Cannizzo, E. Dumas, A. Chaussé, Fabrication and characterization of all-covalent nanocomposite functionalized screen-printed voltammetric sensors, Electrochim. Acta 133 (2014) 467-474. https://doi.org/10.1016/j.electacta.2014.04.069.

[48] V. Meucci, S.L. aschi, M. Minunni, C. Pretti, L. Intorre, G. Soldani, M. Mascini, An optimized digestion method coupled to electrochemical sensor for the determination of

Cd, Cu, Pb and Hg in fish by square wave anodic stripping voltammetry, Talanta 77 (2009) 1143-1148. https://doi.org/10.1016/j.talanta.2008.08.008.

[49] S. Bouden, N. Bellakhal, A. Chaussé, C. Vautrin-Ul, Performances of carbon-based screen-printed electrodes modified by diazonium salts with various carboxylic functions for trace metal sensors, Electrochem. Commun. 41 (2014) 68-71. https://doi.org/10.1016/j.elecom.2014.01.028.

[50] D. Riman, D. Jirovsky, J. Hrbac, M.I. Prodromidis, Green and facile electrode modification by spark discharge: bismuth oxide - screen printed electrodes for the screening of ultra-trace Cd(II) and Pb(II), Electrochem. Commun. 50 (2015) 20-23. https://doi.org/10.1016/j.elecom.2014.11.003.

[51] P. Niu, C. Fernández-Sánchez, M. Gich, C. Navarro-Hernández, P. Fanjul-Bolado, A. Roig, Screen-printed electrodes made of a bismuth nanoparticle porous carbon nanocomposite applied to the determination of heavy metal ions, Microchim. Acta 183 (2016) 617-623. https://doi.org/10.1007/s00604-015-1684-4.

[52] Y. Zhao, L. Xu, S. Li, "One-drop-of-blood" electroanalysis of lead levels in blood using a foam-like mesoporous polymer of melamine-formaldehyde and disposable screen-printed electrodes, Analyst 140 (2015) 1832-1836. 10.1039/C5AN00039D.

[53] M.A. Deshmukh, R. Celiesiute, A. Ramanaviciene, M.D. Shirsat, A. Ramanavicius, EDTA_PANI/SWCNTs nanocomposite modified electrode for electrochemical determination of copper (II), lead (II) and mercury (II) ions, Electrochim. Acta 259 (2018) 930-938. https://doi.org/10.1016/j.electacta.2017.10.131.

[54] M.A. Deshmukh, G.A. Bodkhe, S. Shirsat, A. Ramanavicius, M.D. Shirsat, Nanocomposite Platform Based on EDTA Modified Ppy/SWNTs for the Sensing of Pb(II) Ions by Electrochemical Method, Front. Chem. 6 (2018) 451. https://doi.org/10.3389/fchem.2018.00451.

1. Yeast/Co_3O_4/Au are reported as SPE modifiers for Pb^{2+} determination

2. The resulting LOD is 3.45×10^{-15} g/L with linear range from 10^{-8} g/L to 10^{-14} g/L.

3 Peak current by SWV correlated negatively with Pb^{2+} at lower concentrations

4. The sensing system is simple, low cost and accurate for the detection of Pb^{2+}